European Journal of Medicinal Chemistry 258 (2023) 115539

Contents lists available at ScienceDirect

European Journal of Medicinal Chemistry

journal homepage: www.elsevier.com/locate/ejmech

Research paper

Quinolone analogues of benzothiazinone: Synthesis, antitubercular structure-activity relationship and ADME profiling

Phelelisiwe S. Dube [a], Lesetja J. Legoabe [a,*], Audrey Jordaan [b], Lester Sigauke [a], Digby F. Warner [b], Richard M. Beteck [a,*]

[a] Centre of Excellence for Pharmaceutical Sciences, North-West University, Potchefstroom, 2520, South Africa
[b] Molecular Mycobacteriology Research Unit, Department of Pathology and Institute of Infectious Disease and Molecular Medicine, University of Cape Town, Observatory, 7925, South Africa

ARTICLE INFO

Keywords:
DprE1
Quinolone
Nitro compounds
Mycobacterium tuberculosis
Benzothiazinone

ABSTRACT

Mycobacterium tuberculosis (Mtb) has an impermeable cell wall which gives it an inherent ability to resist many antibiotics. DprE1, an essential enzyme in Mtb cell wall synthesis, has been validated as a target for several TB drug candidates. The most potent and developmentally advanced DprE1 inhibitor, PBTZ169, is still undergoing clinical development. With high attrition rate, there is need to populate the development pipeline. Using a scaffold hopping strategy, we imprinted the benzenoid ring of PBTZ169 onto a quinolone nucleus. Twenty-two compounds were synthesised and screened for activity against Mtb, with six compounds exhibiting sub micromolar activity of MIC_{90} <0.244 μM. Compound **25** further demonstrated sub-micromolar activity when evaluated against wild-type and fluoroquinolone-resistant Mtb strains. This compound maintained its sub-micromolar activity against a DprE1 P116S mutant strain but showed a significant reduction in activity when tested against the DprE1 C387S mutant.

1. Introduction

Tuberculosis (TB) is a communicable disease caused by the bacterium *Mycobacterium tuberculosis* (Mtb). Before the advent of COVID-19, TB was recognized globally as the leading infectious disease originating from a single agent [1]. In 2020, 1.5 million TB related deaths occurred across the globe. This TB death toll is nearly twice that reported for HIV/AIDS (0.68 million) in the same year [2]. The COVID-19 pandemic, the rise in both multi-drug resistant (MDR)-TB and extensively drug-resistant (XDR)-TB have erase years of global progress made in controlling TB, and together they have led to an increase in the number of TB-related deaths [1]. Notably, the overall TB death toll in 2020 was higher than that reported during 2018, and it represents a 5.6% increase relative to 2005 TB death toll [3]. Therefore, TB continues to be a global health issue, and more novel antituberculosis medications are required to effectively keep this disease under control.

The cell wall of Mtb is renowned for being complex, impermeable, and hydrophobic, thus serving as an impenetrable barrier that makes Mtb naturally resistant to numerous antibiotics [4]. Since the discovery of Mtb in 1882, numerous enzymes in cell wall synthesis and maintenance have been validated as essential therapeutic targets [5]. One such target is Decaprenylphosphoryl-β-D-ribose 2′ epimerase (DprE1), a flavoenzyme localised in the periplasmic space of Mtb's cell wall [6,7]. In Mycobacteria and Corynebacterineae species, DprE1 catalyses the conversion of decaprenylphosphoryl-D-ribose (DPR) to decaprenylphosphoryl- 2-Ketoribose (DPX), which is subsequently converted to decaprenylphosphoryl- β-D-arabinose (DPA) (Scheme 1). DPA is the only source of arabinose sugars, an essential monomer needed for the syntheses of arabinogalactan, and subsequently cell wall formation [8]. This makes DprE1 an essential and attractive drug target. The absence of DprE1 in humans further emphasises this enzyme as a suitable drug target [9].

Several new TB drug candidates currently in different stages of development have been validated to act against DprE1 [7]. They belong to diverse compound classes such as aminoquinolones, benzothiazoles, quinaxolines, nitro benzamides, benzothiazinones (BTZs), *etc* (Chikhale et al., 2018). Nitro benzamides and BTZs (Fig. 1) are notable in that they possess sub-micromolar activity against all strains of Mtb, including the strains that cause MDR-TB and XDR-TB [10]. Furthermore, nitro benzamides and BTZs also act as suicide inhibitors of this enzyme. Within

* Corresponding authors.
E-mail addresses: lesetja.legoabe@nwu.ac.za (L.J. Legoabe), 25159194@nwu.ac.za, richmbi1@yahoo.com (R.M. Beteck).

https://doi.org/10.1016/j.ejmech.2023.115539
Received 28 April 2023; Received in revised form 31 May 2023; Accepted 31 May 2023
Available online 9 June 2023

DprE1, the nitro moiety of BTZs and nitro benzamides is reduced to an electrophilic nitroso moiety using electrons from flavin adenine dinucleotide (FAD). The nitroso bearing intermediate then forms a covalent bond with residue Cys387, and permanently inhibits DprE1 [6].

Due to the sub-micromolar MIC values of its derivatives against Mtb, the BTZ scaffold has gained the interest of scientists and researchers working in the field of antimycobacterial agents [11]. PBTZ169, also known as macozinone, is the most developmentally advanced BTZ derivative [12]. Although PBTZ169 is void of chiral centres, and has better pharmacokinetic (PK) properties than its predecessor, BTZ043, it stills suffers from poor PK characteristics, high lipophilicity (clogP:5.1), and low aqueous solubility (<1 μM) [13,14]. As a result, new nitro-based compounds are being investigated as DprE1 suicide inhibitors [15].

Quinolone derivatives are often first choice chemotherapeutics for the management of a variety of bacterial infections, suggesting this scaffold has good PK properties [16]. Modifications in the quinolone basic structure have generated derivatives that inhibit diverse biological targets [17]. For example, quinolone derivatives have been reported to elicit numerous pharmacological effects, including antibacterial, antiviral, antiparasitic, anti-inflammatory, anticholinesterase, anticonvulsant, anticancer, neuroprotective, and diuretic action [18].

In an effort to identify new DprE1 suicide inhibitors to populate the development pipeline, we previously synthesised nitro-quinolones with potent anti-Mtb activity. Molecular docking analyses suggested that the interaction made by the most potent compound within the enzyme active site is similar to those observed with other DprE1 inhibitors [19,20]. The active site residues includes His-132, Gly-133, Lys-134, Leu-317, Val-365, Lys-367, Phe-369, Cys-387 and Lys-418 [21].

In our quest to generate novel DprE1 suicide inhibitors with improved metabolic stability and aqueous solubility, we herein hopped the benzenoid ring of benzothiazinones onto the quinolone nucleus (Fig. 2). While keeping the hopped benzenoid ring intact, we appended amide moieties at positions 3 of the quinolone nucleus. Secondary amides are polar, and metabolically robust. The amide chain length was varied to generate analogues for eventual structure-activity relationship analyses. The clogP values of all synthesised compounds were calculated and compared against PBTZ169 using chemdraw software. Synthesised compounds were screened *in vitro* against an Mtb H37Rv:*gfp* reporter strain, with most compounds demonstrating sub-micromolar activity. Selected compounds (**24**, **25**, **26**) were evaluated against wild-type Mtb H37Rv as well as fluoroquinolone-resistant and *dprE1* mutant Mtb strains. These compounds (**24**, **25**, **26**) were also evaluated for aqueous solubility, and metabolic stability in the presence of human, rat, and mouse liver microsomes.

2. Results and discussion

2.1. Chemistry

In previous work, the nitro group was appended at position C-6, a hydrogen at position C-8, benzyl moieties at position N1, and aliphatic amides at C-3 of the quinolone ring. In this study, the C-6, and C-8 bear a trifluoromethyl, and a nitro moiety, respectively to mimic the benzenoid ring of BTZ. Derivatizations were made at C-3, distal to the NO_2 moiety, to make it freely accessible for subsequent covalent bond formation with the target.

Our target compounds were obtained following a 4-step synthetic route presented in Scheme 2. The first step was the condensation of diethyl ethoxymethylenemalonate with 3-nitro-4-(trifluoromethyl) aniline (**5**), followed by intramolecular cyclisation at 245–250 °C to obtain compound **6** in 80% yields. Compound **6** then underwent saponification, leading to compound **7** in 70%. Compound **7** underwent three more chemical transformations. The first transformation was decarboxylation at 245–250 °C to afford compound **8.** This was followed by bromination using *N*-bromosuccinamide as the bromine source to afford compound **9** in 60% yields. The second transformation involved concurrent chlorination and amidation in refluxing $SOCl_2$ to furnish compound **10**. The third was amide coupling using HATU as a coupling reagent at room temperature to afford target compounds **11**–**27** in 50–70% yields.

The synthesised quinolones were characterized using ^{1}H NMR, ^{13}C NMR, and high-resolution mass spectrometry (HRMS). On the ^{1}H NMR spectra, protons signals were verified based on their chemical shifts, multiplicities and coupling constants. The amine proton (-NH) at N-1 of the quinolone ring appeared as a singlet signal at *ca* 12 ppm. The amide proton at C-3 appeared as triplet at *ca* 9.5–10.5 ppm, with a coupling constant of approximately 6. This amide signal was absent in compounds **6**, **7**, **8**, **9**, since they do not have the amide moiety at C-3. For ^{13}C NMR spectra, the signals appearing at *ca* 177–178 is assignable to the ketone carbon (C=O) at C-4. The amide carbon (CONH) at C-3 appeared at *ca* 159–163 ppm. HRMS analyses confirmed the expected molecular ion for all compounds.

Reagents and conditions: (i) (a) Ethanol, reflux, 24 h, (b) Diphenyl ether, 240 °C, 3 h; (ii) LiOH, THF: H_2O (2:1), reflux, 24 h; (iii) Diphenyl ether, 260 °C, 15 min; (iv), *N*-bromosuccinimide, DMF, 80 °C, 3–5 h; (v) Thionyl chloride, chloroform, reflux, 24 h; (vi) Amine (5 eq), HATU (2eq), TEA (3 eq), DMF, rt, 72 h.

2.2. Pharmacology

2.2.1. Screening against the Mtb H37Rv::gfp reporter strain

Compounds (**6**–**11**, **17**–**27**) were screened *in vitro* for antimycobacterial activity against the Mtb H37Rv*::gfp* reporter strain cultured in Middlebrook 7H9 broth supplemented with either casitone (CAS), glucose and tyloxapol, or albumin, dextrose, catalase (ADC) and Tween 80. Rifampicin, a first line antimycobacterial agent was included in the assay as a reference. The antimycobacterial activity was reported as the minimum concentration required to inhibit 90% (MIC_{90}) of bacterial growth. The MIC_{90} was evaluated on days 7 and 14 following incubation of Mtb with target compounds. No precipitation was observed during screening and compounds were soluble in screening media except for compounds **12**–**16**. The antimycobacterial activity data are summarised in Table 1. Seventeen out of twenty-two compounds

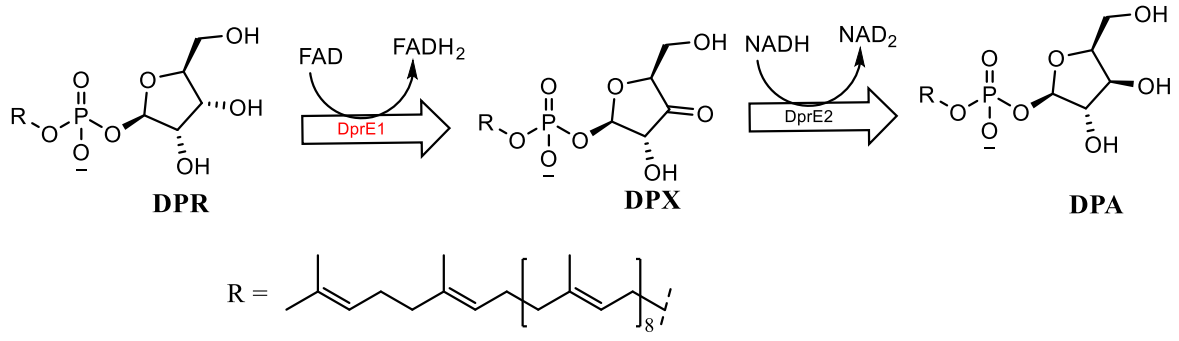

Scheme 1. DprE1 initiated arabinogalactan synthesis.

were screened for activity, five compounds were not soluble in dimethyl sulfoxide (DMSO) and as such no data is provided for them. Sixteen out of seventeen compounds evaluated were active against Mtb, exhibiting activities in the range of <0.244–31.25 μM in ADC-supplemented media.

For some compounds, antimycobacterial activity varied with the different screening media supplements. For example, apart from compounds **7** and **11**, all evaluated compounds displayed activity in the range of <0.244–31.25 μM in ADC-supplemented medium, with compound **27** exhibiting sub-micromolar activity of <0.244 μM. Four of these compounds (**18**, **19**, **21**, **27**) showing good activity in ADC-supplemented medium displayed no antimycobacterial activity when the CAS-supplemented broth medium was used. Compound **8** demonstrated moderate activity of 16 μM in ADC enriched medium, while it exhibited week activity of 62 μM in CAS medium. The fluctuating activity with changing growth medium supplement is attributed to the binding affinity of the supplements with test samples, or how the supplements affect bacteria growth and aggregation. The tween 80 in ADC enriched medium prevents aggregation, acts as a nutrient source that promotes growth of Mtb and hence expression of drug targets. This increases Mtb's susceptibility in the presence of viable inhibitors [22,23].

Other compounds showed better antimycobacterial activity in CAS-supplemented medium than in ADC medium. For example, compounds **9**, **10**, **20**, **23** had potent antitubercular activity in CAS containing medium, but this activity reduced six-fold in ADC supplemented medium. This reduced activity in ADC supplemented medium could be attributed to binding of test samples to albumin, which reduces effective concentration of the sample available to engage the target. This posits that compounds **9**, **10**, **20**, **23** will likely suffer from high protein binding *in vivo*. For compounds **6**,**17**, **25**, **24**, and **26**, antimycobacterial activity did not fluctuate with culture media supplements. These compounds possessed sub-micromolar activity in both culture media.

To allow for proper structure-activity relationship (SAR) and/or structure-property relationship analyses (SPR), the C-3 position of the quinolone nucleus was derivatized with different moieties including H, Br, COOH, ethyl ester, hydrazinamide, amides of varying chain length and phenyl substitution pattern.

The amide derivatives could be grouped into three subseries based on the number of sp^3 carbons located between the phenyl and the amide moieties. The first subseries of 6 compounds (**10**, **12**–**16**) has no sp^3 carbon between the phenyl and the amide moiety. Except compound **10**, this subseries was generally insoluble in DMSO, hence their biological properties were not investigated. The second subseries of seven compounds (**17**–**23**) has one sp^3 carbon between the phenyl and the amide moieties, while the third subseries (**24**–**27**) has two sp^3 carbons. Moreover, the substituents (Cl, F, CF_3, CH_3) attached to the phenyl ring at C-3, and/or their positions (*ortho*, *meta*, and *para*) were also varied to allow SAR analysis.

The activity data indicated that the antimycobacterial activity increased with increase in the number of sp^3 carbons between the phenyl and the amide moieties. Compound **11** bearing a hydrazine moiety was slightly soluble but had no activity at all. All seven compounds (**17**–**23**) from the subseries with 1 sp^3 carbon were soluble in screening media and their antimycobacterial data are included in Table 1. This subseries displayed good activity ranging from the MIC_{90} value of 0.488–15.625 μM. When the number of sp^3 carbons increased to two (**24**–**27**), the activity also increased and the sub-micromolar activity of <0.244 μM was obtained for most of the compounds in both screening media. Two compounds from subseries **24**–**27** were the most active compounds for this study, regardless of the media supplement utilized. This increase in activity with increasing number of sp^3 carbons is evident when comparing compound **21** (1 sp^3 carbon, MIC_{90} 8.1 μM) against **24** (2 sp^3 carbons, MIC_{90} 0.9 μM), and compound **19** (1 sp^3 carbon, MIC_{90} 7.4 μM) against **26** (2 sp^3 carbons, MIC_{90} <0.244 μM). The afore compared compounds differ from one another by one sp^3 carbon only. Increase in sp^3 carbons likely promoted flexibility of the molecules, which in turn enhanced their permeability across Mtb's cell wall. DprE1 being an intracellular target, factors influencing inhibitors' cell wall permeability will also affect target occupancy, and overall whole cell activity.

Furthermore, the SAR suggests that at C-3, an ester moiety promotes activity better than a proton, bromide, or a carboxylic acid. This is evident when looking at compounds **6**–**9**, wherein **6** bearing an ethyl ester has sub micromolar activity of MIC_{90} <0.244 μM, while compounds **7**–**9** possessed MIC_{90} values > 1 μM.

The SAR analysis also indicated that the substitution pattern (*ortho*, *meta*, or *para*) on the phenyl ring within the amide chain also had influence on antimycobacterial activity. It was apparent that substituting the phenyl ring at *ortho* or *meta* position favoured activity, as compared to the *para* position. This is evident when looking at compound **17**, **18**, and **19**; the activity of these compounds fluctuated with the position of chlorine on the phenyl ring. Compound **17**, which has the chlorine atom at *ortho* position exhibited sub micromolar activity in both media, while compounds **18** (chlorine atom at *meta* position) and **19** (chlorine at *para* position) exhibited no activity in CAS supplemented medium and low micromolar activity in ADC supplemented medium. In ADC supplemented medium, compound **18** showed good activity (MIC_{90} 2.9 μM), while its *para* substituted analogue (**19**, MIC_{90} 7.4 μM) exhibited moderate activity. In addition, comparing compounds **20** (fluorine at *meta* position) and **21** (fluorine at *para* position) also evidently show that substituting the *meta* position favours activity over the *para* position. Compound **20** exhibited sub micromolar activity 0.49 μM (CAS medium) and 3.012 μM (ADC medium), but **21** was inactive against Mtb in CAS

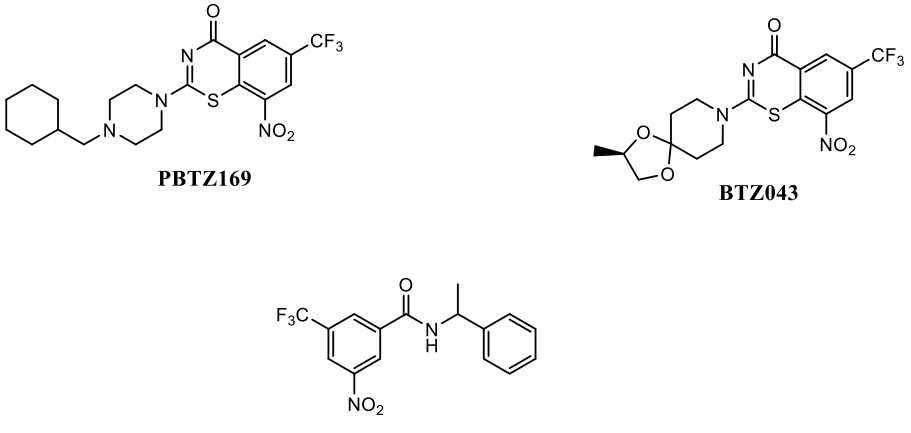

Fig. 1. Nitro compound with potent antitubercular activity.

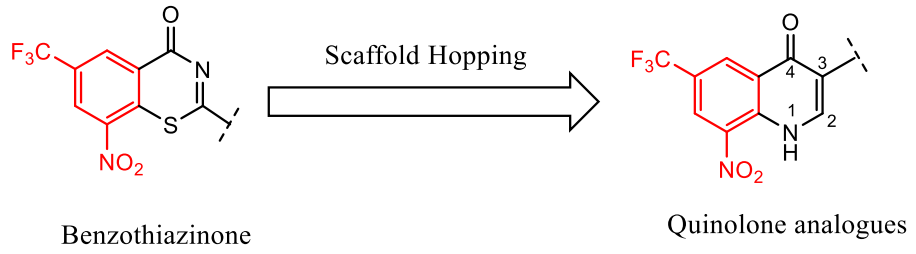

Fig. 2. Scaffold hopping strategy.

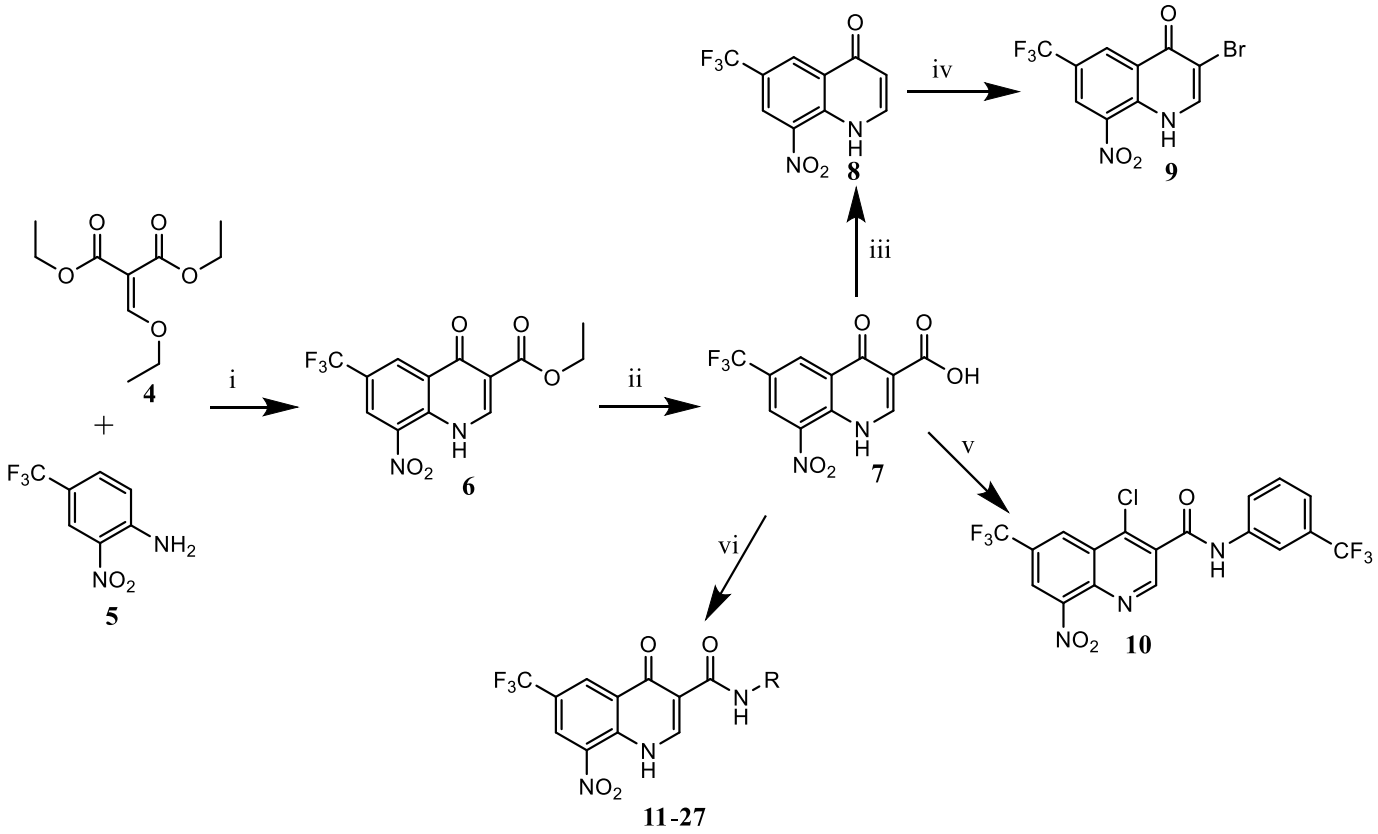

11, R = NH_2
12, R = 2-Cl-phenyl
13, R = 3-Cl-phenyl
14, R = 3-CF_3-phenyl
15, R = 3-F-phenyl
16, R = 3,4-dimethylphenyl

17, R = 2-Cl-benzyl
18, R = 3-Cl-benzyl
19, R = 4-Cl-benzyl
20, R = 3-F-benzyl
21, R = 4-F-benzyl
22, R = 3,4-diF-benzyl
23, R = 3-methylbenzyl

24, R = 1-F-4-ethylphenyl
25, R = 1-CF_3-4-ethylphenyl
26, R = 1-Cl-4-ethylphenyl
27, R = 1-CH_3-4-ethylphenyl

Scheme 2. Synthesis of target compounds.

medium and had good activity (8.107 μM) in ADC medium.

2.2.2. Screening against wild type, and mutant strains of H37Rv

Compounds **24**–**26** were selected and screened against Mtb H37Rv, fluoroquinolone-resistant strain (GyrA_G88C), and two *dprE1* (P116S, and C387S) mutant strains cultured in standard Middlebrook 7H9 ADC. Isoniazid (INH), and moxifloxacin (MOX) were included as references. The selected compounds demonstrated potent activities against the wild-type and fluoroquinolone-resistant strains of Mtb, exhibiting MIC_{90} values in the range of 0.9–2 μM. Unlike moxifloxacin, these compounds maintained their potency against fluoroquinolone-resistant Mtb mutant (Table 2), strongly suggesting that DNA gyrase was not the target – in contrast to the fluoroquinolones. Compounds **24** and **25** further showed no shift in MIC_{90} values against the Mtb DprE1-P116S mutant. In contrast, the three compounds showed significant shift (>4 fold) in MIC_{90} values against DprE1-C387S mutant strain. This lower activity against the DprE1-C387S mutant strain suggests these compounds are DprE1 suicide inhibitors. Mtb bearing the P116S phenotype is resistant

Table 1
In vitro antimycobacterial activity, clogP and structure of target compounds.

Entry	Structure	clogP	MIC_{90} (μM) VS Mtb on day 14	
			CAS, GLU, TX	ADC, GLU, TW
6	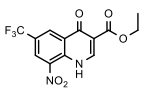	1.6	<0.244	<0.244
7	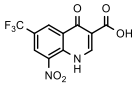	1.8	62.5	>125
8	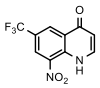	1.0	62.5	16.0
9	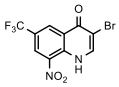	1.9	1.6	16.0
10	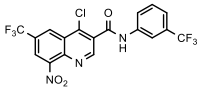	4.8	0.7	31.2
11	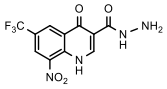	0.1	>125	>125
12	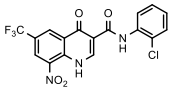	2.2	–	–
13	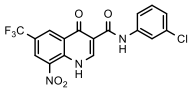	2.2	–	–
14	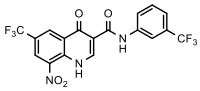	3.6	–	–
15	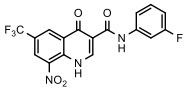	2.5	–	–
16	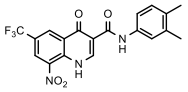	3.3	–	–
17	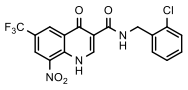	3.2	0.5	0.8
18	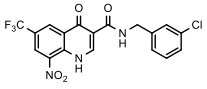	3.2	>125	2.99
19	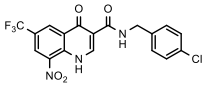	3.2	>125	7.4
20	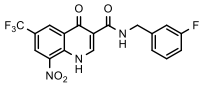	2.6	0.5	3.0
21	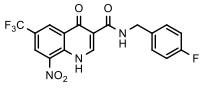	2.6	>125	8.1
22	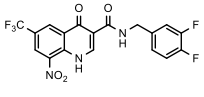	2.7	7.0	31.3

Table 1 (*continued*)

Entry	Structure	clogP	MIC_{90} (μM) VS Mtb on day 14	
			CAS, GLU, TX	ADC, GLU, TW
23	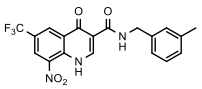	3.0	<0.244	2.9
24	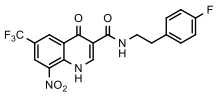	2.8	<0.244	0.9
25	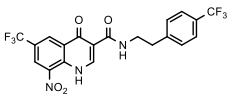	3.5	<0.244	<0.244
26	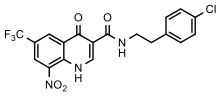	3.4	<0.244	<0.244
27	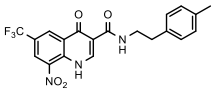	3.1	>125	0.244
RIF	–	–	0.01	0.01

RIF = Rifampicin.
[a]clogP values calculated with chem draw professionals.
[b]MIC_{90} = determined *in vitro* against gfp *Mtb* strain, RF = rifampicin.

Table 2
In vitro activity of compounds **24**–**26** against HEK293, H37Rv, and mutant strains.

Compound	Anti-tubercular activity, (MIC_{90}, μM)				Toxicity, (CC_{50}, μM)
	H37Rv	MoxR	DprE1-P116S	DprE1-P116S	HEK293
24	2.0	1.9	1.0	>62	>20
25	0.9	0.9	0.5	54.2	>20
26	1.9	1.9	17	44.8	>20
INH	3.5	3.6	2.0	3.3	nd
MOX	0.1	6.3	0.1	0.05	nd

MoxR = Moxifloxacin resistant, nd = not determined.

to DprE1 non-covalent inhibitors, while the C387S phenotype is not susceptible to DprE1 covalent inhibitors such as PBTZ169.

The three compounds were evaluated *in vitro* against HEK293 cell line for toxicity, with CC_{50} values of >20 μM.

2.3. ADME profiling

Three compounds (**24**–**26**) were selected, and their aqueous solubility, lipophilicity, and metabolic stability evaluated, Table 3. The three compounds had lipophilicity at pH 7.4 (logD) of <5. These values fall within the acceptable logD range for orally available drugs.

These selected compounds were also evaluated for kinetic aqueous solubility at pH 6.5. All compounds had poor solubility of <5 μM.

Metabolic stability of compounds **24**, **25**, and **26** was determined in the presence of human, rat, and mouse liver microsomes. These compounds all showed moderate metabolic stability. Compound **26**, the most stable, had a % remnant of >75% in all three species after 30 min; while compound **25**, the least stable, had a % remnant of >67% in all three species. Compound **26**, had moderate intrinsic clearance values in the range of 18–24 μl/min/mg in these species.

Table 3
In vitro ADME properties of selected compounds.

Entry	Solubility (μM)	LogD	% remnant at 30 min (HLM/RLM/MLM)	CL_{int}, (μl/min/mg) (HLM/RLM/MLM)
24	<5	4.0	73/75/56	25.9/23.4/48.8
25	<5	4.4	68/68/67	31.7/33.2/33.3
26	<5	4.3	75/80/76	24.3/18.4/23.0

HLM = Human liver microsomes, RLM = Rat liver microsomes, MLM = Mouse liver microsomes. CL_{int} = intrinsic clearance.

2.4. Molecular docking

The induced-fit docking (IFD) workflow predicted and extracted the lowest binding poses of compound **25** within the DprE1 active site. This compound had favourable interactions with the active site based on its IFD score of −939.55. The pose of **25** suggests that a combination of aryl linker flexibility and electronegativity of the ring contribute to a stable IFD pose. A combination of *pi-pi* stacking with aromatic residues, hydrogen bonding, salt bridges between charged groups, halogen bonding, and *pi*-cation interactions are recruited by compound **25** in its interaction with the active site of DprE1 protein.

The docked poses of the ligand in the active site were subjected to MD simulations to explicitly observe the role that water plays in the stability of the interactions over time. Snapshots of representative poses of **25** acquired from the stable region, demonstrated that a lower nitro-sulfhydryl distance of 3.96 Å was stabilized by the presence of additional hydrogen bonds and salt bridge interactions with the tail of the ligand (Fig. 3A). This pose recruits a hydrogen bond to an explicit solvent species in addition to two hydrogen bonds at the nitro group. One of these hydrogen bond interactions occur directly between the sulfhydryl group of Cys387 and the oxygen atom on the nitro group of the ligand (Fig. 3B). This interaction justifies the increased proximity and provides evidence of the likelihood of this pose being adopted by compound **25**.

3. Conclusion

Herein, we further explored the antimycobacterial activity of nitroquinolones-3-carboximides. The synthesised compounds exhibited potent antimycobacterial activity against the Mtb H37Rv:*gfp* reporter strain in the range of <0.244–62.5 μM. Moreover, 6 compounds exhibited sub-micro molar activity of <0.244 μM, which was a great improvement form our previous work. The SAR demonstrates that the number of sp^3 carbons shows a remarkably gradation of activity, each additional CH_2 group on the benzyl amide moiety contributes a fair increment to the antimycobacterial activity of the compound. In addition, the antimycobacterial activity was greatly influence by the position (*para* < *meta* < *ortho*) of benzyl substituents.

Further activity profiling of three lead compounds from this study clearly suggests this compound class as potent DprE1 suicide inhibitors. These compounds maintained potent activity against both wild type and fluoroquinolone resistant strains of Mtb. They demonstrated a significant drop in activity against DprE1-C387S mutant strain of Mtb. Overall, all the target compounds exhibited high antimycobacterial activity, and has the potential to be exploited in the development of new drugs for TB.

4. Materials and methods

4.1. General information

Chemicals and solvents used in this study were purchased from various chemical vendors, including Sigma-Aldrich (Pty) Ltd. (Johannesburg, South Africa), Merck (Pty) Ltd. (Johannesburg, South Africa), Ambeed, AK Scientific, and they were used as supplied. Reactions were monitored using thin layer chromatography (TLC) on Merck $60F_{254}$ silica gel plates (Merck, Johannesburg, South Africa) supported on aluminium. Developed TLC plates were visualized under ultraviolet (UV254 and 366 nm) light or stained with iodine vapour. ^{1}H and ^{13}C NMR spectra were recorded on Bruker Biospin 600 MHz spectrometer, and the chemical shifts are given in values referenced to deuterated dimethylsulfoxide (DMSO-d_6) and are reported in parts per million (ppm). Chemical shifts for deuterated DMSO-d_6 appear at 2.5 and 39.5

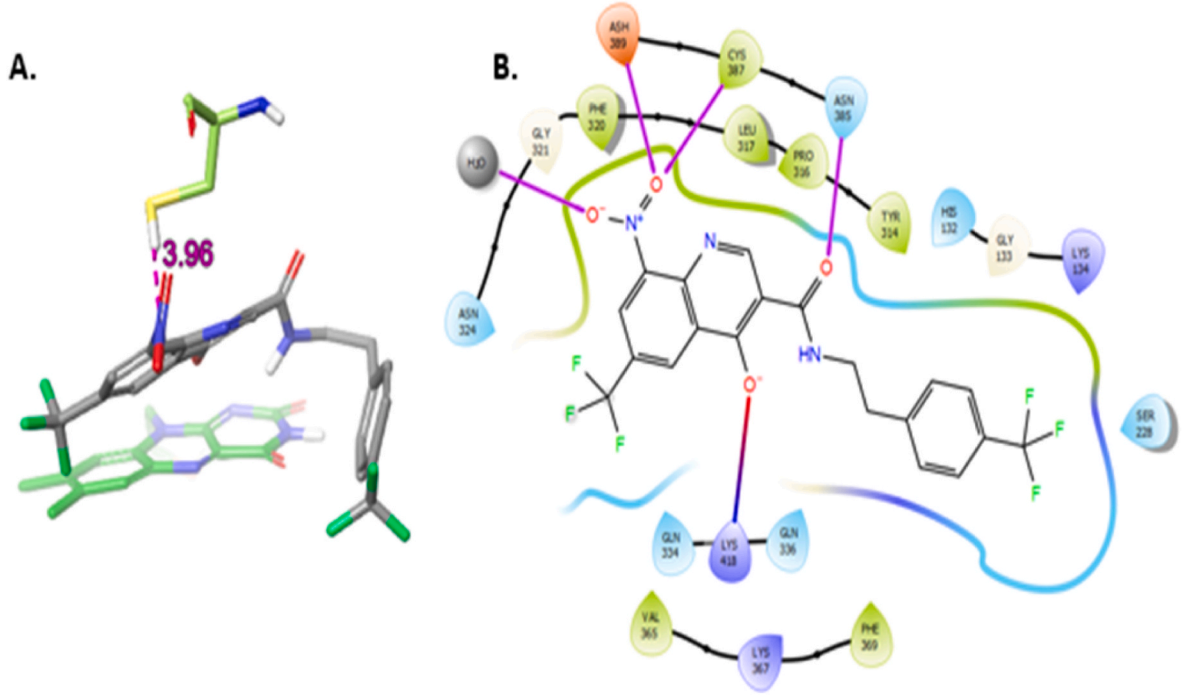

Fig. 3. Representative stable pose of **25** acquired during 100ns of Desmond NPT simulations.

ppm for ^{1}H and ^{13}C NMR spectra, respectively. Proton coupling patterns are abbreviated as follows: s (singlet), d (doublet), t (triplet), q (quartet), and m (multiplet). Coupling constants (*J*) are reported in Hz. NMR data were analysed using MestReNova Software, version 5.3.2e4936. Melting points (mp) were established with a Büchi melting point B-545 instrument. The High-resolution mass spectra (HRMS) were recorded by means of a Bruker micrOTOF-Q II mass spectrometer using atmospheric pressure chemical ionization (APCI) in positive ion mode.

4.2. General synthetic procedure for the nitro-quinolone derivatives

Target compounds were obtained through the synthetic procedures listed below:

a. Generation of the quinolone nucleus

Into a round bottom flask was added 5 g (24 mmol) of 2-nitro-4-trifluoromethyl aniline, diethylethoxymethylenemalonate (1 eq), and 15 mL of ethanol. The mixture was stirred under reflux for 24 h. Upon reaction completion, the mixture was cooled to room temperature, and petroleum ether added to initiate precipitation. The ensued precipitate was filtered, washed again with petroleum ether, then allowed to dry. The dried crude product was then added to boiling Dowtherm A and the mixture heated at 240–260 °C for 3 h to afford compound **6**.

b. Ester hydrolysis

Compound **6** was added to a round bottom flask, followed by LiOH (3 eq), H_2O/THF (1:2), and the mixture refluxed for 24 h. Upon reaction completion as indicated by TLC analyses, the mixture was concentrated and a few drops of HCl added. The mixture was stirred for 10–15 min, and the resulting precipitate filtered, and dried to obtain intermediate **7**.

c. Amide formation

In a around bottom flask was added 0.7 g (2.3mmoles) of **7**, HATU (3 equiv), TEA (3 equiv), and 15 mL of dimethylformamide (DMF). The mixture was stirred at room temperature (rt) for 30–45 min, then appropriate amines (5 equiv) were added, and the mixture further stirred for 3–4 days. Upon completion, the products were purified through silica gel column chromatography using dichloromethane (DCM) as mobile phase, and later recrystallized from ethanol at very low temperatures overnight. The resulting crystals or precipitate were then filtered out of ethanol and dried to obtain compounds **12**–**27**.

4.2.1. Ethyl 8-nitro-4-oxo-6-(trifluoromethyl)-1,4-dihydroquinolone-3-carboxylate, **6**

Yellow powder, yield: 90%, mp: 256 °C. ^{1}H NMR (600 MHz, DMSO-d_6) δ 12.34 (s, 1H-NH), 8.85 (s, 1H-Ar), 8.75 (s, 1H-Ar), 8.61 (s, 1H-Ar), 4.27 (q, J = 7.1 Hz, 2H-CH_2), 1.27 (t, J = 7.1 Hz, 3H-CH_3). ^{13}C NMR (151 MHz, DMSO-d_6) δ 171.36, 163.43, 146.84, 137.77, 135.45, 129.80, 129.41, 126.28, 123.72, 123.49, 112.42, 60.27, 14.13. HRMS APCl *m/z* calcd for $C_{13}H_{10}F_3N_2O_5$ $[M+H]^+$, 331.0536, found: 331.0229.

4.2.2. 8-Nitro-4-oxo-6-(trifluoromethyl)-1,4-dihydroquinolone-3-carboxylic acid, **7**

Light brown powder, yield 75%, mp: 253–255 °C. ^{1}H NMR (600 MHz, DMSO-d_6) δ 8.95 (s, 1H-OH), 8.84 (s, 1H-NH), 7.41–7.37 (m, 1H-Ar), 7.14 (t, J = 7.4 Hz, 1H-Ar), 7.02–6.98 (m, 1H-Ar). ^{13}C NMR (151 MHz, DMSO-d_6) δ 176.14, 164.87, 156.49, 147.92, 129.89, 128.95, 127.05, 123.27, 118.45, 110.14. HRMS-APCl *m/z* calcd for $C_{11}H_6F_3N_2O_5$ [M+H], 303.0223, found: 303.0217.

4.2.3. 8-Nitro-6-(trifluoromethyl)quinolon-4(1H)-one, **8**

Yellow powder, yield: 82%, mp: 193 °C.^{1}H NMR (600 MHz, DMSO-d_6) δ 12.06 (s, 1H-NH), 8.79 (d, J = 2.1 Hz, 1H-Ar), 8.70 (d, J = 2.1 Hz, 1H-Ar), 8.03 (d, J = 7.6 Hz, 1H-Ar), 6.33 (d, J = 7.6 Hz, 1H-Ar). ^{13}C NMR (151 MHz, DMSO-d_6) δ 142.12, 136.15, 129.88, 127.59, 125.59, 123.84, 122.04, 121.72, 118.44, 111.32. HRMS-APCl *m/z* calc for $C_{10}H_6F_3N_2O_3$ $[M+H]^+$, 259.0325, found: 259.0326.

4.2.4. 3-Bromo-8-nitro-6-(trifluoromethyl)quinolon-4(1H)-one, **9**

Brown powder, yield: 87%, mp: 201–203 °C. ^{1}H NMR (600 MHz, DMSO-d_6) δ 12.35 (s, 1H-NH), 8.87 (d, J = 2.0 Hz, 1H-Ar), 8.40 (d, J = 11.4 Hz, 1H-Ar), 7.60–7.54 (m, 1H-Ar). ^{13}C NMR (151 MHz, DMSO-d_6) δ 171.00, 142.20, 138.14, 138.14, 136.10, 133.19, 130.74, 126.27, 122.64, 122.64. HRMS APCl *m/z* calcd for $C_{10}H_5BrF_3N_2O_3$ $[M+H]^+$, 336.9430, found: 336.9417.

4.2.5. 4-Chloro-8-nitro-6-(trifluoromethyl)-N-(3-(trifluoromethyl)phenyl) quinolone-3-carboxamide, **10**

Cream powder, yield: mp: 270 °C. ^{1}H NMR (600 MHz, DMSO-d_6) δ 11.29 (s, 1H-NH), 9.39 (s, 1H-Ar), 9.02 (d, J = 1.8 Hz, 1H-Ar), 8.88 (d, J = 0.9 Hz, 1H-Ar), 8.27 (d, J = 6.0 Hz, 1H-Ar), 8.04–7.80 (m, 1H-Ar), 7.67 (t, J = 8.0 Hz, 1H-Ar), 7.56 (d, J = 7.8 Hz, 1H-Ar). ^{13}C NMR (151 MHz, DMSO-d_6) δ 162.64, 153.63, 149.30, 141.05, 140.70, 139.49, 132.16, 130.86, 126.33, 123.83, 121.41, 116.25. HRMS APCl *m/z* calcd for $C_{18}H_9ClF_6N_3O_3$ $[M+H]^+$, 464.0175, found: 464.0191.

4.2.6. 8-Nitro-4-oxo-6-(trifluoromethyl)-1,4-dihydroquinolone-3-carbohydrazide, **11**

Grey powder, yield: 71%, mp: 258 °C. ^{1}H NMR (600 MHz, DMSO-d_6) δ 12.72 (s, 1H-NH), 8.78 (s, 1H-NH), 8.01 (s, 1H-Ar), 7.77 (d, J = 1.8 Hz, 1H-Ar), 7.26 (d, J = 1.8 Hz, 1H-Ar), 6.18 (s, 2H-NH_2). ^{13}C NMR (151 MHz, DMSO-d_6) δ 175.76, 160.01, 153.37, 143.52, 140.00, 129.31, 126.44, 110.87, 110.17, 108.89. HRMS-APCl *m/z* calcd for $C_{11}H_8F_3N_4O_4$ $[M+H]^+$, 315.0962, found: 315.0945. Purity (HPLC): 96.9%.

N-(2-chlorophenyl)-8-nitro-4-oxo-6-(trifluoromethyl)-1,4-dihydroquinolone-3-carboxamide, **12**. Yellow powder, yield 80%, mp 364–365 °C. HRMS-APCl *m/z* calcd for $C_{17}H_{10}ClF_3N_3O_4$ $[M+H]^+$, 412.0306 found: 412.0283.

N-(3-chlorophenyl)-8-nitro-4-oxo-6-(trifluoromethyl)-1,4-dihydroquinolone-3-carboxamide, **13**. Yellow powder, yield 88%, mp 363–365 °C. HRMS-APCl *m/z* calcd for $C_{17}H_{10}ClF_3N_3O_4$ $[M+H]^+$, 412.0306 found: 412.0286.

4.2.7. 8-Nitro-4-oxo-6-(trifluoromethyl)-N-(3-(trifluoromethyl)phenyl)-1,4-dihydroquinolone-3-carboxamide,**14**

Yellow powder, yield 80%, mp 358 °C. ^{1}H NMR (600 MHz, DMSO-d_6) δ 12.87 (s, 1H-NH), 11.91 (s, 1H-NH), 8.94–8.69 (m, 3H-Ar), 8.24 (s, 1H-Ar), 7.74 (d, J = 8.1 Hz, 1H-Ar), 7.57 (t, J = 7.9 Hz, 1H-Ar), 7.44 (d, J = 7.7 Hz, 1H-Ar). ^{13}C NMR (151 MHz, DMSO-d_6) δ 174.57, 161.47, 146.78, 138.63, 137.93, 134.91, 130.06, 129.64, 127.93, 126.70, 123.16, 120.13, 115.61, 112.55. HRMS-APCl *m/z* calcd for $C_{18}H_{10}F_6N_3O_4$ $[M+H]^+$, 446.0552 found: 446.0570.

4.2.8. N-(3-fluorophenyl)-8-nitro-4-oxo-6-(trifluoromethyl)-1,4-dihydroquinolone-3-carboxamide, **15**

Rust powder, yield 85%, mp 349 °C. ^{1}H NMR (600 MHz, DMSO-d_6) δ 12.89 (s, 1H-NH), 11.91 (s, 1H-NH), 8.97–8.87 (m, 3H-Ar), 7.82–7.72 (m, 1H-Ar), 7.39 (dd, J = 4.1, 7.3 Hz, 2H-Ar), 6.95 (t, J = 8.4, 2.5 Hz, 1H-Ar). ^{13}C NMR (151 MHz, DMSO-d_6) δ 174.33, 161.07, 146.69, 130.21 (d, J^{CF} = 9.5 Hz), 127.70, 121.96, 115.03, 112.33, 106.26, 106.08. HRMS-APCl *m/z* calcd for $C_{17}H_{10}F_4N_3O_4$ $[M+H]^+$, 396.0602 found: 396.0583.

4.2.9. N-(2,3-dimethylphenyl)-8-nitro-4-oxo-6-(trifluoromethyl)-1,4-dihydroquinolone-3-carboxamide, **16**

Yellow powder, yield 82%, mp 344–345 °C. HRMS-APCl *m/z* calcd for $C_{19}H_{15}F_3N_3O_4$, $[M+H]^+$, 406.1009 found: 406.0986.

4.2.10. N-(2-chlorobenzyl)-8-nitro-4-oxo-6-(trifluoromethyl)-1,4-dihydroquinolone-3-carboxamide, **17**

Yellow powder, yield 51%, mp 235–237 °C. ^{1}H NMR (600 MHz, DMSO-d_6) δ 12.73 (s, 1H-NH), 9.96 (t, J = 6.0 Hz, 1H-NH), 8.95–8.81 (m, 3H-Ar), 7.51–7.45 (m, 1H-Ar), 7.45–7.38 (m, 1H-Ar), 7.34–7.29 (m, 2H-Ar), 4.63 (d, J = 6.0 Hz, 2H-CH$_2$). ^{13}C NMR (151 MHz, DMSO-d_6) δ 174.49, 162.81, 146.23, 137.91, 135.96, 135.09, 132.22, 129.77, 129.19 (d, J^{CF} = 9.9 Hz), 128.83, 128.27, 127.21, 126.54, 123.58, 123.36, 113.00, 40.33. HRMS-APCl m/z calcd for $C_{18}H_{12}ClF_3N_3O_4$ $[M+H]^+$, 426.0463, found: 426.65. Purity (HPLC): 100%.

4.2.11. N-(3-chlorobenzyl)-8-nitro-4-oxo-6-(trifluoromethyl)-1,4-dihydroquinoline-3-carboxamide, **18**

Yellow powder, yield 65%, mp 207 °C. ^{1}H NMR (600 MHz, DMSO-d_6) δ 12.70 (s, 1H-NH), 9.90 (t, J = 6.0 Hz, 1H-NH), 8.91 (d, J = 2.0 Hz, 1H-Ar-H), 8.89–8.83 (m, 2H-Ar-H), 7.40–7.30 (m, 4H-Ar-H), 4.58 (d, J = 6.0 Hz, 2H-CH$_2$). ^{13}C NMR (151 MHz, DMSO-d_6) δ 174.50, 162.93, 146.28, 141.84, 137.95, 135.14, 132.99, 130.22, 129.81, 128.38, 127.11, 126.80, 126.55, 125.98, 123.41, 113.21, 41.73. HRMS-APCl m/z calcd for $C_{18}H_{12}ClN_3O_4$ $[M+H]^+$, 426.0463, found: 426.0458. Purity (HPLC): 99.5%.

4.2.12. N-(4-chlorobenzyl)-8-nitro-4-oxo-6-(trifluoromethyl)-1,4-dihydroquinolone-3-carboxamide,**19**

Yellow powder, yields 66%, mp 240 °C. ^{1}H NMR (600 MHz, DMSO-d_6) δ 12.66 (s, 1H-NH), 9.86 (t, J = 5.9 Hz, 1H-NH), 8.90 (d, J = 1.9 Hz, 1H-Ar), 8.87 (s, 2H-Ar), 7.38 (d, J = 4.8 Hz, 4H-Ar), 4.57 (d, J = 6.0 Hz, 2H-CH$_2$). ^{13}C NMR (151 MHz, DMSO-d_6) δ 174.42, 162.76, 146.12, 138.12, 137.83, 135.00, 131.37, 129.72, 129.07, 128.37 (d, J^{CF} = 15.9 Hz), 128.12 (d, J^{CF} = 17.8 Hz), 126.41, 113.24, 41.54. HRMS-APCl m/z calcd for $C_{18}H_{12}ClN_3O_4$ $[M+H]^+$, 426.0463, found: 426.0448. Purity (HPLC): 98.5%.

4.2.13. N-(3-fluorobenzyl)-8-nitro-4-oxo-6-(trifluoromethyl)-1,4-dihydroquinolone-3-carboxamide, **20**

Yellow powder, yield 59%, mp 254 °C. ^{1}H NMR (600 MHz, DMSO-d_6) δ 12.73 (s, 1H-NH), 9.98 (t, J = 5.9 Hz, 1H-NH), 8.86–8.74 (m, 3H-Ar), 7.42–7.34 (m, 1H-Ar), 7.25–7.17 (m, 1H-Ar), 7.15 (dd, J = 10.2, 2.2 Hz, 1H-Ar), 7.07 (td, J = 8.4, 2.3 Hz, 1H-Ar), 4.59 (d, J = 6.0 Hz, 2H-CH$_2$). ^{13}C NMR (151 MHz, DMSO-d_6) δ 174.03, 162.91, 162.68, 161.06, 146.74, 141.93 (d, ^{CF}J = 7.1 Hz), 135.51, 129.94 (d, J^{CF} = 8.3 Hz), 129.10, 128.14, 125.52, 122.90 (d, J^{CF} = 2.7 Hz), 113.68, 113.53, 113.30, 113.16, 112.76, 41.44. HRMS-APCl m/z calcd for $C_{18}H_{12}F_4N_3O_4$ $[M+H]^+$, 410.0758, found:410.0746. Purity (HPLC): 99%.

4.2.14. N-(4-fluorobenzyl)-8-nitro-4-oxo-6-(trifluoromethyl)-1,4-dihydroquinolone-3-carboxamide, **21**

Orange powder, yield 40%, mp 257 °C.^{1}H NMR (600 MHz, DMSO-d_6) δ 12.70 (s, 1H-NH), 9.87 (t, J = 5.9 Hz, 1H-NH), 8.91 (d, J = 2.1 Hz, 1H-Ar), 8.86–8.84 (m, 2H-Ar), 7.45–7.33 (m, 2H-Ar), 7.22–7.10 (m, 2H-Ar), 4.55 (d, J = 5.9 Hz, 2H-CH$_2$). ^{13}C NMR (151 MHz, DMSO-d_6) δ 174.80, 163.09, 162.29, 160.69, 146.57, 138.30, 135.64 (d, J^{CF} = 3.0 Hz), 135.47, 130.06, 129.66 (d, J^{CF} = 8.2 Hz), 128.65, 126.83, 123.91, 123.68, 115.46, 115.32, 113.54, 41.85. HRMS-APCl m/z calcd for $C_{18}H_{12}F_4N_3O_4$ $[M+H]^+$, 410.0758, found: 410.0746. Purity (HPLC): 99.8%.

4.2.15. N-(3,4-difluorobenzyl)-8-nitro-4-oxo-6-(trifluoromethyl)-1,4-dihydroquinolone-3-carboxamide, **22**

Mustard powder, yield 50%, mp 260 °C. ^{1}H NMR (600 MHz, DMSO-d_6) δ 12.70 (s, 1H-NH), 9.90 (t, J = 5.9 Hz, 1H-NH), 8.91 (s, 1H-Ar), 8.85 (d, J = 7.4 Hz, 2H-Ar), 7.44–7.33 (m, 2H-Ar), 7.20 (s, 1H-Ar), 4.54 (d, J = 5.9 Hz, 2H-CH$_2$). ^{13}C NMR (151 MHz, DMSO-d_6) δ 174.81, 163.28, 146.60, 138.29, 135.47, 130.11, 128.68, 126.93, 124.42, 117.65 (d, J^{CF} = 17.0 Hz), 116.70 (d, J^{CF} = 17.1 Hz), 113.50, 41.64. HRMS-APCl m/z calcd for $C_{18}H_{11}F_5N_3O_4$ $[M+H]^+$, 428.0664, found: 428.0648.

4.2.16. N-(3-methylbenzyl)-8-nitro-4-oxo-6-(trifluoromethyl)-1,4-dihydroquinolone-3-carboxamide, **23**

Yellow powder, yield 69%. Mp 212–214 °C.^{1}H NMR (600 MHz, DMSO-d_6) δ 12.71 (s, 1H-NH), 9.85 (t, J = 5.9 Hz, 1H-NH), 8.91 (d, J = 2.1 Hz, 1H-Ar), 8.87–8.84 (m, 2H-Ar), 7.23 (t, J = 7.5 Hz, 1H-Ar), 7.16–7.11 (m, 2H-Ar), 7.07 (t, J = 9.4 Hz, 1H-Ar), 4.53 (d, J = 5.9 Hz, 2H-CH$_2$), 2.29 (s, 3H-CH$_3$). ^{13}C NMR (151 MHz, DMSO-d_6) δ 174.87, 163.03, 146.56, 139.22, 138.30, 137.84, 135.48, 130.15, 128.66 (d, J^{CF} = 2.6 Hz), 128.25, 127.90, 126.89, 124.74, 123.69, 113.58, 42.57, 21.29. HRMS-APCl m/z calcd for $C_{19}H_{15}F_3N_3O_4$ $[M+H]^+$, 406.1009, found: 406.0997. Purity (HPLC): 99.9%.

4.2.17. N-(4-fluorophenethyl)-8-nitro-4-oxo-6-(trifluoromethyl)-1,4-dihydroquinolone-3-carboxamide, **24**

Mustard powder, yield 87%, mp 269 °C. ^{1}H NMR (600 MHz, DMSO-d_6) δ 12.68 (s, 1H-NH), 9.50 (t, J = 5.7 Hz, 1H-NH), 8.90 (d, J = 2.1 Hz, 1H-Ar), 8.84–8.80 (m, 2H-Ar), 7.30 (dd, J = 8.5, 5.7 Hz, 2H-Ar), 7.15–7.08 (m, 2H-Ar), 3.58 (dd, J = 13.0, 7.0 Hz, 2H-CH$_2$), 2.84 (t, J = 7.1 Hz, 2H-CH$_2$). ^{13}C NMR (151 MHz, DMSO-d_6) δ 174.36, 162.62, 161.55, 159.95, 146.04, 137.92, 135.51, 135.21 (d, J^{CF} = 29.4 Hz), 130.31 (d, J^{CF} = 8.0 Hz), 129.72, 128.23, 126.46, 123.63, 123.23, 115.03, 114.89, 113.16, 40.02, 34.18. HRMS-APCl m/z calcd for $C_{19}H_{14}F_4N_3O4$ $[M+H]^+$, found: 424.0898. Purity (HPLC): 97.3%.

4.2.18. 8-Nitro-4-oxo-6-(trifluoromethyl)-N-(4-(trifluoromethyl) phenethyl)-1,4-dihydroquinolone-3-carboxamide, **25**

Mustard powder, yield 85%, mp 270–274 °C. ^{1}H NMR (600 MHz, DMSO-d_6) δ 12.67 (s, 1H-NH), 9.67–9.34 (m, 1H-NH), 8.90 (d, J = 2.1 Hz, 1H-Ar), 8.82 (s, 2H-Ar), 7.67 (t, J = 13.6 Hz, 2H-Ar), 7.50 (d, J = 8.0 Hz, 2H-Ar), 3.64 (dd, J = 13.0, 7.0 Hz, 2H-CH$_2$), 3.02–2.88 (m, 2H-CH$_2$). ^{13}C NMR (151 MHz, DMSO-d_6) δ 174.32, 162.70, 146.09, 144.18, 137.96, 135.13, 129.48 (d, J^{CF} = 41.4 Hz), 129.33, 128.22, 126.35, 125.04 (d, J^{CF} = 3.8 Hz), 123.20, 113.11, 34.81. HRMS-APCl m/z calcd for $C_{20}H_{14}F_6N_3O_4$ $[M+H]^+$, 474.0883 found: 474.0873. Purity (HPLC): 98.9%.

4.2.19. N-(4-chlorophenethyl)-8-nitro-4-oxo-6-(trifluoromethyl)-1,4-dihydroquinolone-3-carboxamide, **26**

Mustard powder, yield 82%, mp 262 °C. ^{1}H NMR (600 MHz, DMSO-d_6) δ 12.67 (s, 1H-NH), 9.50 (t, J = 5.7 Hz, 1H-NH), 8.90 (d, J = 2.1 Hz, 1H-Ar), 8.83–8.81 (m, 2H-Ar), 7.39–7.32 (m, 2H-Ar), 7.31–7.27 (m, 2H-Ar), 3.59 (dd, J = 12.9, 7.0 Hz, 2H-CH$_2$), 2.90–2.81 (m, 2H-CH$_2$). ^{13}C NMR (151 MHz, DMSO-d_6) δ 174.34, 162.62, 146.03, 138.19, 137.90, 135.09, 130.69, 130.38, 129.67, 128.19 (d, J^{CF} = 9.3 Hz), 126.41, 113.14, 39.92, 34.30. HRMS-APCl m/z calcd for $C_{19}H_{14}ClF_3N_3O_4$ $[M+H]^+$, 440.0575 found: 440.0608. Purity (HPLC): 97.9%.

4.2.20. N-(4-methylphenethyl)-8-nitro-4-oxo-6-(trifluoromethyl)-1,4-dihydroquinolone-3-carboxamide, **27**

Yellow powder, yield 85%, mp 272 °C. ^{1}H NMR (600 MHz, DMSO-d_6) δ 12.67 (s, 1H-NH), 9.49 (t, J = 5.6 Hz, 1H-NH), 8.90 (d, J = 2.1 Hz, 1H-Ar), 8.85–8.80 (m, 2H-Ar), 7.15 (d, J = 8.0 Hz, 2H-Ar), 7.13–7.07 (m, 2H-Ar), 3.57 (dd, J = 13.0, 7.1 Hz, 2H-CH$_2$), 2.80 (t, J = 7.2 Hz, 2H-CH$_2$), 2.26 (s, 3H-CH$_3$). ^{13}C NMR (151 MHz, DMSO-d_6) δ 174.34, 162.55, 145.97, 137.85, 135.99, 135.00 (d, J^{CF} = 16.9 Hz), 129.71, 128.83, 128.28 (d, J^{CF} = 16.4 Hz), 126.40, 123.60, 123.21, 113.20, 40.09, 34.62, 20.49. HRMS APCl m/z calcd for $C_{20}H_{17}F_3N_3O_4$ $[M+H]^+$, 420.1166, found: 420.1151. Purity (HPLC): 96.3%.

4.3. In vitro antimycobacterial assay

The *in vitro* antimycobacterial evaluation was done following the procedure by Beteck et al. (2019). A 10 mL culture of Mtb pMSp12::*gfp*

was grown to an optical density ($0D_{600}$) of 0.6–0.7. The cultures were grown in standard Middlebrook 7H9 medium supplemented with albumin, dextrose, catalase (ADC) and 0.05% Tween80, or in Middlebrook 7H9 medium supplemented with 0.03% casitone (CAS), 0.4% glucose, and 0.05% tyloxapol and diluted 1:500 prior to inoculation. The compounds to be tested were then reconstituted to a 10 mM stock in DMSO. Two-fold serial dilutions of the test compounds were plated in 96 well plates and 50 μL of the diluted Mtb culture were then added to each well. Rifampicin (2 x MIC) was used as a minimum growth control for assay and 5% DMSO as the maximum growth control. The microtitre plates were sealed in a secondary container and incubated at 37 °C with 5% CO_2 and humidification. Fluorescence readings (excitation 485 nM; emission 520 nM) obtained for the individual wells were measured using a plate reader (FLUOstar OPTIMA, BMG LABTECH) at day 14. The raw fluorescence data was analysed using the CDD Vault from Collaborative Drug Discovery, in which data was normalized to the minimum and maximum inhibition controls to generate a dose response curve (% inhibition). Using the Levenberg-Marquardt damped least squares method, the minimum inhibitory concentration (MIC) was calculated. The lowest concentration of drug/test compound that inhibited growth of more than 90% of the bacterial population was considered the MIC_{90}.

4.4. In vitro cytotoxicity evaluation

HEK-293 cells were grown using Dulbecco's Modified Eagle Medium (DMEM) supplemented with 10% foetal bovine serum (FBS). The cells were plated in compound-containing plates at a density of 5×10^3 cells per well, and a volume of 50 μL. The plates were incubated for 20 h at 37 °C in 5% CO_2. Resazurin, 5 μL, was added to each well and the plates were further incubated for 3 h.

Plates were excited at 560 nm, and the emission of each well measured at 590 nm using a Tecan M1000 Pro monochromator plate reader. The CC_{50} (concentration required to inhibit 50% cell growth) value was generated by computing the inhibition values against the corresponding log [concentration] using a sigmoidal dose-response function with variable fitting values for the bottom, top, and slope. Any value with a $>$ indicates samples with CC_{50} values above the maximum tested concentration (32 μg/mL).

4.5. Solubility determination

Aqueous solubility was determined in 96-well plate format at pH 6.5 and making use of an adapted miniaturised shake-flask method. From a 10 mM stock of the sample prepared in DMSO was collected 4 μL, which was added to a 96-well plate and evaporated using a GeneVac system. This was followed by addition of phosphate buffer saline (pH 6.5) to the compounds containing wells, and plates incubated for 24 h at 25 °C while shaking. The plates were centrifuged at 3500 g for 15 min, and then transferred to an analysis plate. Concentrations of 10–220 μM in DMSO were prepared for each sample, and used to generate a calibration curve from which the solubility of each sample was determined. Analyses were performed by HPLC-DAD [24].

4.6. $LogP_{7.4}$ determination

Lipophilicity at pH 7.4 (LogD) was determined in 96-well plate format using a miniaturised shake-flask method. To each compound in a deep-well plate was added equal volumes of 1-octanol and Phosphate buffered saline (pH 7.4). The plate was vigorously shaken for 2 h at 25 °C, and the phases were carefully separated into different plates for analysis. Analysis was performed by HPLC-UV (Agilent 1200 rapid resolution HPLC coupled to a Diode Array Detector). Log D values were determined from the peak areas of the compound in octanol and buffer phases [24].

4.7. Metabolic stability testing

Compounds were incubated at 1 μM in human (mixed gender, Xenotech), Rat (male rat IGS, Xenotech) and mouse (male mouse CD1, Xenotech) liver microsomes (0.4 mg/mL) at 37 °C for 30 min, followed by addition of ice-cold acetonitrile containing internal standard to quench the reaction. Samples were centrifuged, and then analysed by LC-MS/MS for the disappearance of parent compound. Half-life, clearance and hepatic excretion ratios were determined using standard equations [24].

4.8. Molecular modelling

For the interrogation of the small molecule with the DprE1 receptor using molecular modelling, the CT319 bound protein was acquired from the PDB database through the 4FD0 access code [25]. Compound **25** was constructed using the Marvin Sketch web tool. The Maestro Protein Preparation Wizard with the following parameters (assigning bond orders, adding hydrogens to workspace structure, creating relevant disulphide bonds, generating ionization/tautomeric states for all het groups, optimizing H-bonds, and deleting all waters, system prepared using PROPKA at pH 7) was used to prepare the protein receptor for docking. The ligand was treated with the LigPrep workflow using the following parameters (hydrogens added and pH of 7.0 and a maximum of 32 stereoisomers for each ligand) [26]. Starting conformations for Desmond molecular dynamic simulations were acquired from an Induced-Fit Docking (IFD) workflow of the small molecule ligand (Miller et al., 2021). The IFD workflow docked the ligand within a box centred around the CT319 ligand (OT5 ligand). The following steps were carried out during the IFD workflow: protein preparation (rmsd 0.18), glide docking (sp, 20 poses per ligand, opls2005), determine residues determination and refinement (distance cut-off of 5.0 å), prime active site optimization (opls2005), scoring and filtering (filter using prime energy, energy window of 30 kcal/mol, keep maximum of 20 poses per ligand), glide docking2 (xp, 1 pose per ligand, opls2005), and scoring (prime energy). The pose with the lowest prime energy score for ligand receptor complex was the starting conformation for the molecular dynamic (MD) simulations. The same IFD workflow parameters were used to re-dock the CT319 ligand in the original crystal structure protein. The reliability of the docking protocol was assessed by monitoring the proximity of the ligand's nitro group from the sulphur atom of the Cys 387 residue.

MD simulations of the ligand were performed using the Desmond simulation [27]. The systems were prepared in an orthorhombic box of buffer size 10 Å, solvated by TIP3P waters, and neutralized by adding sodium ions. The OPLS5 forcefield was used for system preparation. Prior to the start of the 100 ns of NPT unrestrained production simulations, the standard NPT relaxation protocol was used to get each system to a temperature of 300 K and an isotropic pressure of 1.013 bar. The distances between the sulphur atom of the Cys387 residue and the nitro group of the ligands during the simulations were monitored.

Declaration of competing interest

The authors declare that they have no known competing financial interests or personal relationships that could have appeared to influence the work reported in this paper.

Data availability

Data is presented in the manuscript as well as the supporting file

Acknowledgement

This project is funded by NWU, faculty of health sciences through research grant awarded to RMB. PSD, LJL, RMB are grateful to North-West University, South Africa for financial support. We appreciate Dr

D. Otto, and Dr J. Jordaan of Chemical Resource Beneficiation unit, Potchefstroom, South Africa for generation of NMR and HRMS data. Research reported in this publication was supported by the South African Medical Research Council with funds received from the Department of Science and Innovation (to DFW). DFW also acknowledges the financial support of the Research Council of Norway (R&D Project 261669 "Reversing antimicrobial resistance"). Metabolic stability studies, antimycobacterial activity against mutant Mtb strains were conducted at H3D on service basis.

Appendix A. Supplementary data

Supplementary data to this article can be found online at https://doi.org/10.1016/j.ejmech.2023.115539.

List of abbreviation used

Mtb	mycobacterium tuberculosis
TB	tuberculosis
HIV	human immunodeficiency virus
AIDS	acquired immunodeficiency syndrome
MDR	multi-drug resistant
XDR	extensively drug-resistant
DprE1	Decaprenylphosphoryl-β-D-ribose 2'epimerase
DPR	Decaprenylphosphoryl-β-D-ribose
DPX	Decaprenylphosphoryl-2-ketoribose
BTZs	benzothiazinones
FAD	flavin adenine dinucleotide
MIC	minimum inhibitory concentration
PK	pharmacokinetic properties
HATU	1-[bis(dimethylamino)methylene]-1H-1,2,3-triazolo [4,5-b]-pyridinium 3-oxid hexafluorophosphate
HRMS	high-resolution mass spectrometry
CAS	casitone
ADC	albumin, dextrose, catalase
DMSO	dimethyl sulfoxide
SAR	structure-activity relationship
SPR	structure-property relationship
INH	isoniazid
MOX	moxifloxacin
ADME	absorption, distribution, metabolism, and excretion
IFD	induced-fit docking
DMEM	Dulbecco's modified eagle medium
FBS	Foetal bovine serum
HPLC-UV	high-performance liquid chromatography-ultraviolet

References

[1] WHO, WHO Global Lists of High Burden Countries for Tuberculosis (TB), TB/HIV and Multidrug/rifampicin-Resistant TB (MDR/RR-TB), 2021–2025: Background Document, 2021. https://apps.who.int/iris/handle/10665/341980 on 31.01.2023.
[2] WHO, Guidelines: Updated Recommendations on HIV Prevention, Infant Diagnosis, Antiretroviral Initiation and Monitoring, 2021. https://apps.who.int/iris/handle/10665/340190 on 31.01.2023.
[3] Z. Stojanovic, F. Goncalves-Carvalho, A. Marin, J.A. Dominguez, I. Latorre, A. Lacoma, et al., Advances in diagnostic tools for respiratory tract infections: from tuberculosis to COVID-19–changing paradigms? ERJ Open. Res. 9 (2022) 1–5.
[4] R. Tiwari, U. Mollmann, S. Cho, S.G. Franzblau, P.A. Miller, M.J. Miller, Design and syntheses of anti-tuberculosis agents inspired by BTZ043 using a scaffold simplification strategy, ACS Med. Chem. Lett. 5 (2014) 587–591.
[5] K. Duncan, C.E. Barry III, Prospects for new antitubercular drugs, Curr. Opin. Microbiol. 7 (2004) 460–465.
[6] R.V. Chikhale, M. A Barmade, P. R Murumkar, M. R Yadav, Overview of the development of DprE1 inhibitors for combating the menace of tuberculosis, J. Med. Chem. 61 (2018) 8563–8593.
[7] M. Brecik, I. Centarova, R. Mukherjee, G.S. Kolly, S. Huszar, A. Bobovska, E. Kilacskova, et al., DprE1 is a vulnerable tuberculosis drug target due to its cell wall localization, ACS Chem. Biol. 10 (2015) 1631–1636.
[8] K.N. Mikusová, H. Huang, T. Yagi, M. Holsters, D. Vereecke, W. D'Haeze, M. S. Scherman, et al., Decaprenylphosphoryl arabinofuranose, the donor of the D-arabinofuranosyl residues of mycobacterial arabinan, is formed via a two-step epimerization of decaprenylphosphoryl ribose, J. Bacteriol. 187 (2005) 8020–8025.
[9] M. Imran, A.S. Alshrari, H.K. Thabet, M.D. Afroz Bakht Abida, et al., Synthetic molecules as DprE1 inhibitors: a patent review, Expert Opin. Ther. Pat. 13 (2021) 759–772.
[10] K. Lv, X. You, B. Wang, Z. Wei, Y. Chai, B. Wang, A. Wang, et al., Identification of better pharmacokinetic benzothiazinone derivatives as new antitubercular agents, ACS Med. Chem. Lett. 8 (2017) 636–641.
[11] J. Shi, J. Lu, Z. Zong, F. Huo, J. Luo, Q. Liang, Y. Li, et al., In vitro activity of PBTZ169 against multiple Mycobacterium species, Antimicrob. Agents Chemother. 62 (2018), e01314-e01318.
[12] A.O. Mariandyshev, A.L. Khokhlov, S.V. Smerdin, V.S. Shcherbakova, O. V. Igumnova, I. V Ozerova, A.A. Bolgarina, et al., The main results of clinical trials of the efficacy, safety and pharmacokinetics of the perspective anti-tuberculosis drug makozinone (PBTZ169), Ter. Arkh. 92 (2020) 61–72.
[13] G. Zhang, M. Howe, C.C. Aldrich, Spirocyclic and bicyclic 8-nitrobenzothiazinones for tuberculosis with improved physicochemical and pharmacokinetic properties, ACS Med. Chem. Lett. 10 (2019) 348–351.
[14] K. Mikusova, V. Makarov, J. Neres, DprE1–from the discovery to the promising tuberculosis drug target, Curr. Pharm. des. 20 (2014) 4379–4403.
[15] V. Makarov, B. Lechartier, M. Zhang, J. Neres, A.M. van der Sar, S.A. Raadsen, R. C. Hartkoorn, et al., Towards a new combination therapy for tuberculosis with next generation benzothiazinones, EMBO Mol. Med. 6 (2014) 372–383.
[16] P.D. Duarte, M.W. Paixão, A.G. Corrêa, Microwave assisted synthesis of 4-quinolones and N, N'-diarylureas, Green Process. Synth. 2 (2013) 19–24.
[17] P.S. Dube, L.J. Legoabe, R.M. Beteck, Quinolone: a versatile therapeutic compound class, Mol. Divers. 1–26 (2022), https://doi.org/10.1007/s11030-022-10581-8.
[18] P. Dhiman, N. Arora, P.V. Thanikachalam, V. Monga, et al., Recent advances in the synthetic and medicinal perspective of quinolones: a review, Bioorg. Chem. 92 (2019), 103291.
[19] P. S Dube, L.J. Legoabe, A. Jordaan, O. J Jesumoroti, T. Tandamudzimu, D. F. Warner, R.M. Beteck, Easily accessed nitroquinolones exhibiting potent and selective anti-tubercular activity, Eur. J. Med. Chem. 213 (2021), 113207.
[20] R. M Beteck, A. Jordaan, R. Seldon, D. Laming, H. C Hoppe, D.F. Warner, S. D Khanye, Easy-to-access quinolone derivatives exhibiting antibacterial and anti-parasitic activities, Molecules 26 (2021) 1141.
[21] I. Bhutani, S. Loharon, P. Gupta, R. Madathil, R. Parkesh, Structure, dynamics, and interaction of Mycobacterium tuberculosis (Mtb) DprE1 and DprE2 examined by molecular modeling, simulation, and electrostatic studies, PLoS One 10 (2015), e0119771.
[22] R.-D. Pietersen, I. du Preez, M. van Reenen, D. Beukes, G. Leisching, B. Baker, Tween 80 induces a carbon flux rerouting in Mycobacterium tuberculosis, J. Microbiol. Methods 170 (2020), 105795.
[23] C. du Preez, L. J Legoabe, A. Jordaan, O.J. Jesumoroti, D.F. Werner, R.M. Beteck, Arylnitro monocarbonyl curcumin analogues: synthesis and in vitro antitubercular evaluation, Chem. Biol. Drug Des. 101 (2023) 717–726.
[24] P. S Dube, K.T. Angula, L.J. Legoabe, A. Jordaan, J.M. Boitz Zarella, J.S. Doggett, D.F. Werner, R.M. Beteck, Quinolone-3-amidoalkanol: a new class of potent and broad-spectrum antimicrobial agent, ACS Omega 8 (2023) 17086–17102.
[25] S.M. Batt, T. Jabeen, V. Bhowruth, L. Quill, P.A. Lund, L. Eggeling, L.J. Alderwick, et al., Structural basis of inhibition of Mycobacterium tuberculosis DprE1 by benzothiazinone inhibitors, Proc. Natl. Acad. Sci. USA 109 (2012) 11354–11359.
[26] L.L.C. Schrödinger, Schrödinger Release 2022-3, *LigPrep*. Schrödinger, LLC, New York, NY, USA, 2021.
[27] K.J. Bowers, F.D. Sacerdoti, J.K. Salmon, Y. Shan, D.E. Shaw, E. Chow, H. Xu, et al., Molecular dynamics—Scalable algorithms for molecular dynamics simulations on commodity clusters, in: Proceedings of the 2006 ACM/IEEE Conference on Supercomputing-SC'06, ACM Press, 2006.